Soft Matter

PAPER

View Article Online
View Journal | View Issue

Cite this: *Soft Matter*, 2016, **12**, 9622

Electric field makes Leidenfrost droplets take a leap

Sander Wildeman*[a] and Chao Sun*[ba]

Received 30th June 2016,
Accepted 30th October 2016

DOI: 10.1039/c6sm01506a

www.rsc.org/softmatter

Leidenfrost droplets, *i.e.* droplets whose mobility is ensured by a thin vapor film between the droplet and a hot plate, are exposed to an external electric field. We find that in a strong vertical electric field the droplet can start to bounce progressively higher, defying gravitational attraction. From the droplet's trajectory we infer the temporal evolution of the amount of charge on the droplet. This reveals that the charge starts high and then decreases in steps as the droplet slowly evaporates. After each discharge event the charge is in a fixed proportion to the droplet's surface area. We show that this behavior can be accurately modeled by treating the droplet as a conducting sphere that occasionally makes electrical contact with the hot plate, at intervals dictated by an electro-capillary instability in the vapor film. An analysis of the kinetic and potential energies of the bouncing droplet reveals that, while the overall motion is damped, the droplet occasionally experiences a sudden boost, keeping its energy close to the value for which the free fall trajectory and droplet oscillation are in sync. This helps the droplet to escape from the hot surface when finally the electrical surface forces overtake gravity.

Four hundred years ago William Gilbert noticed how a water droplet sitting on a dry surface is "drawn up into a cone" when a piece of statically charged amber is held above it.[1] Important progress on this topic was made a few centuries later: by Lord Rayleigh[2] in his work on the stability limits of charged droplets and by Millikan,[3] who showed in his famous oil-drop experiments that charge is quantized. Closely after, Zeleny[4] published beautiful photographs of how droplets suspended from thin glass capillaries, destabilize when a high voltage is applied between the liquid and a nearby grounded plate. The change of shape of the droplet from a spherical cap to a cone and the subsequent jetting of small charged droplets from the cone tip, were later put on firm theoretical grounds by Taylor.[5] The curious behavior of charged liquid is further exemplified by phenomena like floating water bridges,[6,7] whipping jets,[8,9] and the non-coalescence of oppositely charged drops.[10,11]

An equally curious effect, with uncharged droplets, was demonstrated by Leidenfrost in 1756.[12] He showed that water droplets can survive for seconds on a glowing hot iron spoon, without the instant evaporation one might expect. The effect, occurring above a critical temperature T_L of the spoon, is explained by a thin vapor film sustained below the droplet, which thermally insulates the droplet from the hot metal. The vapor film also enables Leidenfrost droplets to move with very little friction.[13] It has been demonstrated that these hypermobile droplets can be conveniently trapped and steered by equipping the hot surface with ratchet-like structures[14–16] or, in the case of a paramagnetic liquid, by using a magnet.[17] For an overview of the work on Leidenfrost droplets we refer to the review by Quéré.[18]

We bring together the classic experiments of Gilbert and Leidenfrost, and investigate how Leidenfrost droplets behave in a strong electric field. Previously it has been shown that the Leidenfrost state can be suppressed by applying a voltage directly between the hovering droplet and the hot plate.[19,20] In our experiments we apply the electric field externally, so that the forces are determined by a capacitive coupling between the electrodes and the droplet. Similar ideas have been employed to guide droplets through microfluidic devices.[21,22]

1 Setup and method

The setup, shown in Fig. 1, consists of a stainless steel ball ($\varnothing$24 mm) mounted a distance d = 7 mm above a polished aluminum plate. The sphere is connected to a high voltage DC power supply and the bottom plate is grounded. The temperature of the plate can be set *via* an external temperature controller. In each experiment the plate had a constant temperature T well above the Leidenfrost point T_L, and the top electrode was set to a potential V_s between 2 and 5 kV. With a grounded stainless steel needle (not shown) we then gently deposited a millimeter sized droplet of water, ethanol or perfluorohexane (FC72) on the hot

[a] *Physics of Fluids Group, University of Twente, 7500, AE Enschede, The Netherlands. E-mail: swildeman@gmail.com, chaosun@tsinghua.edu.cn*
[b] *Center for Combustion Energy and Department of Thermal Engineering, Tsinghua University, 100084 Beijing, China*

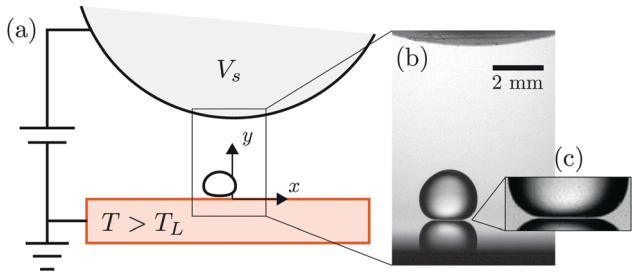

Fig. 1 (a) Schematic of the setup. A droplet hovering on a hot plate ($T > T_L$) is trapped under a spherical electrode set to a high voltage V_s between 2 and 5 kV. (b) Image captured by the high speed camera just after deposition. It shows a millimetric droplet of ethanol and its reflection in the polished aluminum plate. In the magnification of the contact region (c) the thin vapor gap, which insulates the drop from the hot surface, is clearly visible.

Table 1 Relevant vapor (v) and liquid (l) properties used throughout the text. All material parameters are taken at the boiling temperature of the liquid

Property	Sym.	Unit	Ethanol	Water	FC72
Boiling point	T_b	°C	78	100	56
Surface tension	γ	mN m^{-1}	17	59	10
Dielectric permittivity (l)	ε_r	—	19	55	1.7
Density (l)	ρ	kg m^{-3}	730	950	1594
Density (v)	ρ_v	kg m^{-3}	1.6	0.6	12.5
Viscosity (v)	μ_v	μPa s	10	12	12
Thermal conductivity (v)	k_v	W (mK)$^{-1}$	0.02	0.02	0.01
Latent heat	L	kJ kg^{-1}	900	2260	88

plate (see Table 1 for an overview of the relevant liquid properties). The spherical shape of the top electrode ensures that a charged Leidenfrost droplet experiences a small horizontal force that traps the droplet below the center of the sphere (see Appendix A). The droplet's motion was recorded with a high speed camera and the captured frames were further processed with an image analysis script to obtain the center-of-mass (CM) trajectory ($X_{CM}(t)$, $Y_{CM}(t)$) and the volume $\Omega \equiv 4\pi R^3/3$ of the droplet, defining an effective droplet radius R.

2 Vertical droplet trajectory and radius

Fig. 2 shows a recording of an ethanol Leidenfrost droplet ($T = 220$ °C) in a electric field of strength $E = 2.9$ kV cm^{-1} ($V_s = 2$ kV). The first frame shown was taken about 10 seconds after deposition. Initially the droplet bounces with a small amplitude $\Delta Y_{CM} \ll R$. For most parts the amplitude decreases slowly with time. However, as indicated by the upward arrows, it occasionally shows a sudden increase. Interestingly, near the end of the sequence in Fig. 2(b) this behavior reverses. In this final stage the jump height steadily increases in time, now with an occasional drop in amplitude (downward arrows). Finally, it bridges the gap completely and impacts onto the top electrode (Fig. 2 (d)). In Section 5 we will analyze this peculiar motion in detail. However, for this we first need to understand the (dis)charging behavior of the droplet, which will be the focus of Sections 3 and 4.

The full time series of the extracted CM trajectory and the effective radius are shown in Fig. 3(a) (top panel). While the droplet is close to the surface its radius R decreases approximately linear in time. A fit to the first part of the $R(t)$ curve of ethanol in Fig. 3(a) gives $-dR/dt \approx 0.03$ mm s^{-1}. Similar values are found for water ($-dR/dt \approx 0.01$ mm s^{-1}) and FC72 ($-dR/dt \approx 0.08$ mm s^{-1}), increasing in order of liquid volatility (see Fig. 3(c) and (d), respectively). For the ethanol droplet the evaporation rate somewhat decreases in the final stage (stage II in Fig. 3(a)). This is likely due to a combined effect of the lower temperature experienced by the drop (on average it spends less time near the hot plate) and its lower velocity (so that convective contributions to the mass flux are reduced). A proper treatment of the mass and heat transfer problem of an oscillating Leidenfrost droplet

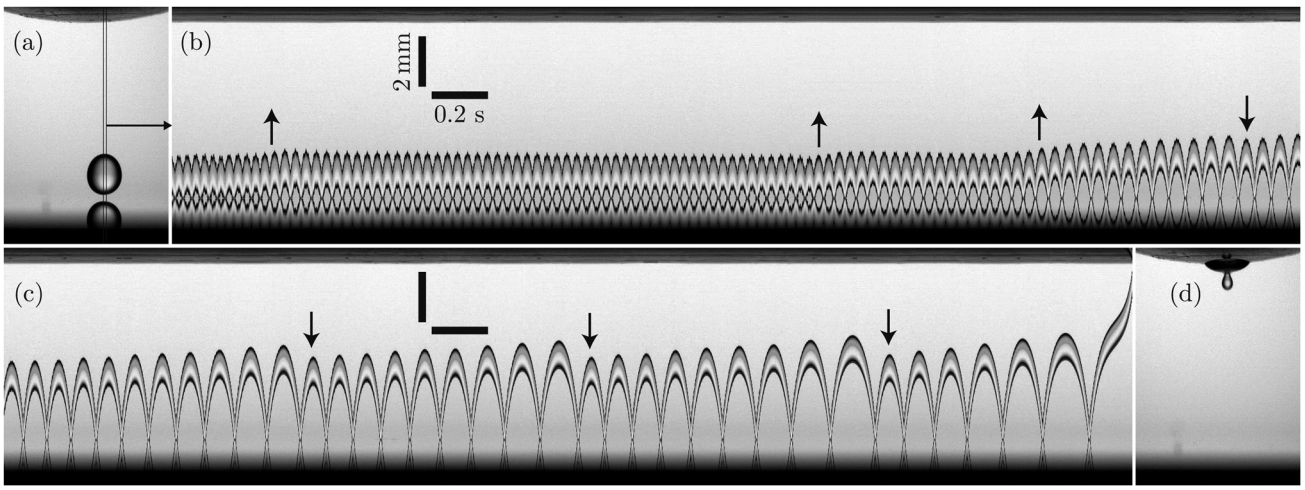

Fig. 2 Typical dynamics of a small Leidenfrost droplet in a strong electric field. Figures (b) and (c) were obtained by taking from each subsequent frame in the high speed recording a thin vertical strip through the center of mass of the droplet (shown in (a) for the first frame) and then merging all these strips. The total time covered by (b and c) is about 9 seconds with a gap of 1 second between the initial stage (b) and the final stage (c). The up- and downward arrows in (b) and (c) indicate the times for which there is a sudden increase or decrease in the jumping amplitude. In (d) the droplet has just impacted on the unheated top electrode, ejecting a small secondary droplet.

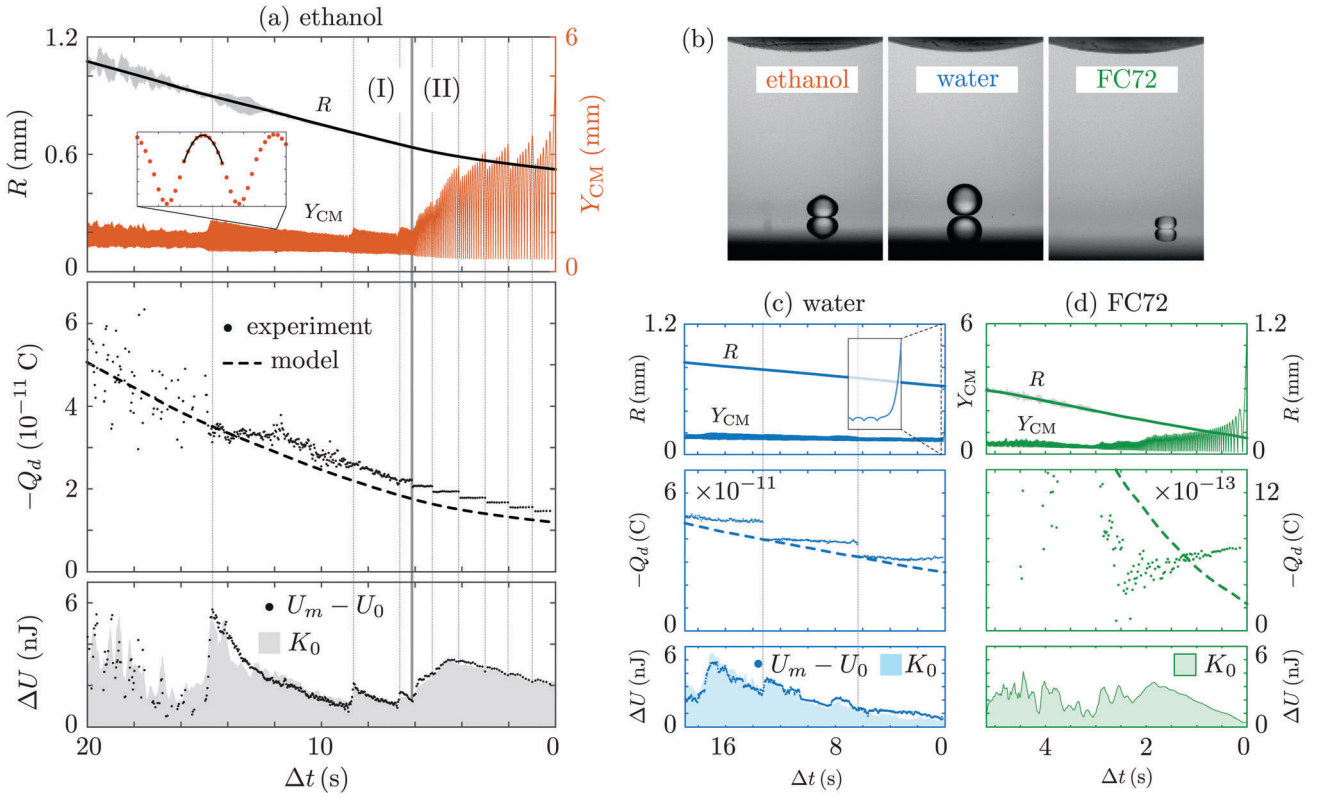

Fig. 3 Extracted dribbling and charging behavior for (a) ethanol, (c) water and (d) FC72 Leidenfrost droplets in an external electric field (with V_s = 2.0 kV, 3.0 kV and 2.5 kV, respectively). For each liquid the time evolution of droplet radius R and vertical trajectory Y_{CM} (top panel), the inferred and predicted droplet charge Q_d (middle panel), and the jumping energy ΔU (bottom panel) are shown. The data for R were smoothed (solid line) to remove non-physical fluctuations in the tracking (gray shading). In (a) the inset shows a magnified region of 70 ms of the trajectory, where a parabola was fitted to one of the peaks to obtain the free-fall acceleration $\ddot{Y}_{CM}$. In (c) the inset on Y_{CM} shows that also the water droplet finally makes it to the top electrode. The solid vertical line in (a) separates the qualitatively different initial (I) and final stage (II) seen for ethanol. The vertical dotted lines in both (a) and (c) serve to correlate key features in the stacked panels such as the charge plateaus and sudden changes in amplitude. For FC72 we took into account its low permittivity by multiplying the prediction for the charge by $f = (\varepsilon_r - 1)/(\varepsilon_r + 2) = 0.2$ (note the different scale on the axis for the charge on the FC72 droplet). Panel (b) shows snapshots of the three tested liquids at their maximal deformation during a rebound.

would require detailed knowledge about the varying conditions outside the droplet (such as temperature, vapor saturation) and the boundary layers that develop. This is outside the scope of this work.

3 Droplet charge

When the droplet is free from the surface the only external forces acting on it are gravity $F_g = -mg$, air drag F_d and electrical forces F_e from the electrodes and image charges, where m is the mass of the droplet and g is the gravitational acceleration. For the small velocities considered here, we can safely neglect the air drag. The vertical component of the equation of motion then takes the form

$$m\ddot{Y}_{CM} = -mg + F_e(Y_{CM}, R, V_s, Q_d), \quad (1)$$

in which Q_d is the charge on the droplet. Since we can measure m, $\ddot{Y}_{CM}$ (see inset Fig. 3(a)), Y_{CM} and R, and we control V_s, we can in principle solve eqn (1) to infer Q_d, given the function $F_e(Y_{CM}, R, V_s, Q_d)$. The simplest form of this function is obtained by assuming that the droplet is a point charge in an external electric field of strength $E = V_s/d$, so that $F_e \approx -Q_d V_s/d$. This point charge model could be extended by including forces $\sim Q^2/(4\pi\varepsilon_0 Y_{CM}^2)$ from image charges in the top and bottom electrode. Although this approach can capture most of the charging trends, it fails when the droplet is close to the electrodes, where it can no longer be considered to be a point. In this case we can view our system as consisting of three finite conductors: a grounded plate, a spherical top electrode and the droplet. For any configuration of conductors at potentials V_i one can write the charge on conductor i as $Q_i = \sum_j c_{ij} V_j$, where the capacitance coefficients c_{ij} only depend on the geometry of the problem, and $c_{ij} = c_{ji}$.[23] The total potential energy for the system can then be written as $U_e = \frac{1}{2}\sum_i Q_i V_i - \sum_n Q_n V_n$. The first sum runs over all conductors and the second sum over all conductors connected to a constant voltage supply. In our experiment the geometry is fully specified by Y_{CM}, R, and the (fixed) position and radius of the top electrode (see Fig. 4). We can therefore write $Q_d = c_{dd}V_d + c_{ds}V_s$ and $Q_s = c_{ss}V_s + c_{sd}V_d$, where the subscripts s and d refer to the top electrode and the droplet, respectively. The charge Q_p on the bottom plate is not relevant here, as $V_p = 0$ and it therefore does

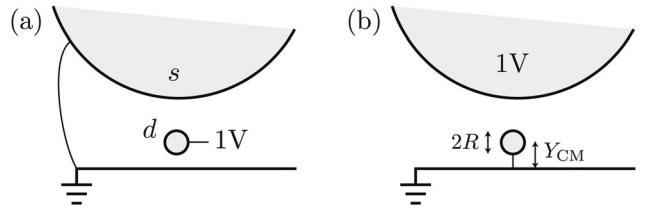

Fig. 4 Canonical electrostatic problems to calculate the capacitance coefficients in our experiment. The height Y_{CM} and radius R of the droplet are varied. From (a) we get $c_{dd}(Y,R) = Q_d$ and $c_{sd}(Y,R) = Q_s$, and in (b) we have $c_{ds}(Y,R) = Q_d$ and $c_{ss}(Y,R) = Q_s$.

not contribute to the potential energy. Using these relations to express $U_e = (Q_d V_d - Q_s V_s)/2$ in terms of Q_d and V_s (which are constant during each flight) one obtains:

$$U_e = \frac{1}{2c_{dd}} Q_d^2 - \frac{c_{ds}}{c_{dd}} Q_d V_s + \frac{1}{2}\left(\frac{c_{ds}^2}{c_{dd}} - c_{ss}\right) V_s^2. \quad (2)$$

Finally, the force needed to vary the droplet height Y_{CM} is found from the principle of virtual work as

$$F_e = -\partial_{Y_{CM}} U_e. \quad (3)$$

The required capacitance coefficients $c_{ij}(Y_{CM}, R)$ have an analytical representation only in some limiting cases (which will be discussed later). For the remaining configurations the coefficients were determined numerically using COMSOL (see Appendix B). Combining eqn (1) through (3) we find a quadratic equation for Q_d, which we solve for each maximum in the droplet's flight trajectory. The numerical capacitance coefficients take into account the precise geometry and configuration of the electrodes and any forces due to induced images charges and dipoles.

As can be seen in Fig. 3(a) (middle panel), the inferred amount of charge on the droplet starts high and then decreases in time as the droplet evaporates. Initially, there is a large scatter in the inferred charge (left of first dotted line). This is mostly related to a similar initial scatter in the measured droplet volume and center of mass position. A likely reason for this apparent scatter is the non-axisymmetric wobbling of the droplet observed in the initial regime (due to capillary waves created during deposition, and possibly by the discharges in the vapor gap). This invalidates the assumption of an axisymmetric droplet shape underlying the image analysis. Another source of error will be the assumption of a spherical droplet shape in the numerical calculation of the capacitance coefficients. We expect the value of the extracted charge to be most reliable in the later stages, when the drop shape closely approximates a sphere. In the final stage, about 6 seconds before impact, the charge decreases in a step-like manner, perfectly correlated with the sudden changes in the jumping amplitude (see vertical lines in region (II) of Fig. 3(a)).

The fact that the charge on the droplet decreases with time, indicates that there is occasionally electrical contact between the droplet and the plate, most likely during a rebound. Irrespective of how this contact occurs we can model the droplet during this stage as a small conducting sphere adhered to a grounded plate (Fig. 4(b) with $Y_{CM} = R$). The problem of finding the charge on the sphere (droplet) is mathematically equivalent to that of finding the polarization of two adhering spheres aligned with an external electric field. This problem has been solved by Smith & Rungis[24] using the method of images, who give the following analytical expression for the amount of charge Q_d on each sphere:

$$Q_d(R) = -\frac{2\pi^3}{3}\frac{\varepsilon_0 R^2 V_s}{d}, \quad (4)$$

where $\varepsilon_0 \approx 8.85 \times 10^{-12}$ F m^{-1} is the vacuum permittivity and we approximated the external field as $-V_s/d$. This is about twice ($2\pi^2/9$ to be precise) the displaced charge one would find for a single sphere of radius R in the same electric field. Taking R from the measurements, we compare eqn (4) to the experimental data in Fig. 3(a) (middle panel). Both magnitude and trend are in good agreement, without any fitting parameters.

4 Discharge mechanism

To understand how the droplet loses its charge, it is insightful to estimate the electric field strength $\sim V_d/H$ in the vapor film during a rebound (where H is the film thickness). The droplet's potential can be expressed as $V_d = (Q_d - c_{ds}V_s)/c_{dd}$, with the coefficients evaluated at $Y_{CM} = R + H$. Since we will have $H \ll R$, we can approximate $c_{ds}(R + H,R)$ as $c_{ds}(R,R)$, which can be directly read off from eqn (4): $c_{ds}(R,R) = -2\pi^3\varepsilon_0 R^2/(3d)$. To find the second coefficient, $c_{dd}(R + H,R)$, we use the geometry in Fig. 4(b), but neglect the top electrode, as it is relatively far away in this case. This classical electrostatics problem[23,25] has the solution $c_{dd}(R+H,R) \approx 4\pi\varepsilon_0 R\left(\gamma + \ln\left(\sqrt{2R/H}\right)\right)$ in the limit $H \ll R$, where $\gamma \approx 0.577$ is the Euler–Mascheroni constant. With this, the potential of the droplet can be written as:

$$V_d \approx -\frac{\pi^2}{6}\frac{R_0^2 - R^2}{R\left[\gamma + \ln\left(\sqrt{2R/H}\right)\right]}\frac{V_s}{d} \quad (H \ll R). \quad (5)$$

Here we assumed that the droplet made its last electrical contact at some radius R_0, obtaining a charge $Q_d(R_0)$ as given by eqn (4). We see that the drop potential is zero after each contact, and becomes negative as R shrinks due to evaporation. The minimum height of the vapor film, appearing in the logarithm in eqn (5), can be estimated by balancing the Laplace pressure $P_\gamma = 2\gamma/R$ exposed in the flattened bottom, with the lubrication pressure P_μ in the vapor flowing out through the small gap.[26] The details of this estimate can be found in Appendix C. For the ethanol droplet under study we find $H \approx 6R^{5/4}\Delta T^{1/4}$ μm, with R given in mm and $\Delta T = T - T_b$. To give an estimate of the maximum value of V_d reached before a discharge event, consider a droplet of initial radius $R_0 = 0.6$ mm that

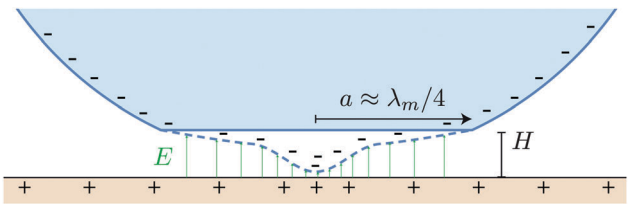

Fig. 5 Cartoon of the electro-capillary instability in the vapor gap that we speculate to be at the root of the observed discharge events.

evaporates by a small amount ΔR to a final radius $R = R_0 - \Delta R$. With $\Delta T \approx 140$ K, we find $H \approx 10$ μm, so that eqn (5) becomes $V_d \approx -1.1 V_s \Delta R/d$. The duration of a charge step in Fig. 3(a) is approximately 1 second. The droplets shrinks by about $\Delta R = 0.02$ mm in this time, so we find $V_d \approx -6$ V at the moment of discharge. Although this gives rise to a strong electric field in the gap, of about 600 kV m^{-1}, it is still far below the breakdown voltage of ethanol vapor $V_b \approx 500$ V for gap sizes of 10 μm at atmospheric pressure.[27]

Another pathway for discharge would be an electro-capillary kind of instability in the vapor gap, akin to the classical cases that can occur for a charged droplet as a whole.[2,5] To investigate this possibility, consider a perturbation $h(x)$ on the flattened bottom of the droplet during a rebound (see Fig. 5 for a sketch of the situation). The pressure distribution at the liquid–vapor interface will have two main contributions: the Laplace pressure $P_l = \gamma\kappa \approx \gamma\partial_x^2 h$ and an electrostatic pressure $P_e = -\frac{1}{2}\varepsilon_0 E^2 \approx -\frac{1}{2}\varepsilon_0[V_d/(H + h(x))]^2 \approx -\frac{1}{2}\varepsilon_0 V_d^2[1 - 2h(x)/H]/H^2$, where in the approximations we used that $h(x) \ll H$ (as is the case when the instability sets in). This situation is similar to the unstable configuration of a dense fluid atop a lighter fluid, for which the Rayleigh–Taylor (RT) instability can set in.[26,28,29] As for the RT-instability, the Laplace pressure stabilizes the interface, while the destabilizing role of the hydrostatic pressure $\rho g h(x)$ is here played by the electrostatic pressure $\varepsilon_0 V_d^2 h(x)/H^3$. From this analogy we can immediately obtain an expression for the smallest unstable wavelength. For the RT-instability we have $\lambda_{RT} = 2\pi\sqrt{\gamma/(\rho g)}$. Replacing ρg by $\varepsilon_0 V_d^2/H^3$ as suggested by the analogy, we obtain:

$$\lambda_m = 2\pi\sqrt{\frac{\gamma H^3}{\varepsilon_0 V_d^2}}. \quad (6)$$

The largest wavelength that can be supported on the bottom of the droplet surface is approximately $\lambda_m \approx 4a$, where a is the radius of the flattened area (that is, half a wavelength over the diameter $2a$). Using this condition in eqn (6) we find a minimum droplet voltage for the onset of the instability as

$$V_c = -\frac{\pi}{2}\sqrt{\frac{\gamma H^3}{\varepsilon_0 a^2}} \quad (7)$$

In the side-view recordings of ethanol droplets we observed that $a \sim R$ during each impact. Using this in eqn (7), we find $V_c \approx -4$ V for $R = 0.6$ mm and $H = 10$ μm, which is indeed close to the value of -6 V inferred from the measurements using eqn (5). Note that λ_m strongly depends on H. This may facilitate a non-linear steepening of the growing mode as the drop's surface is attracted closer to the bottom plate. On the other hand, the strong evaporation in the gap may limit the amplitude of the instability. With the limited spatial and temporal resolution in our setup we were unfortunately not able to directly capture the details of a discharge event, which will be a topic for further investigation.

5 Dribbling motion and escape

From eqn (1) and (4) it is clear that the droplet will eventually jump to the top electrode. The force acting on the surface

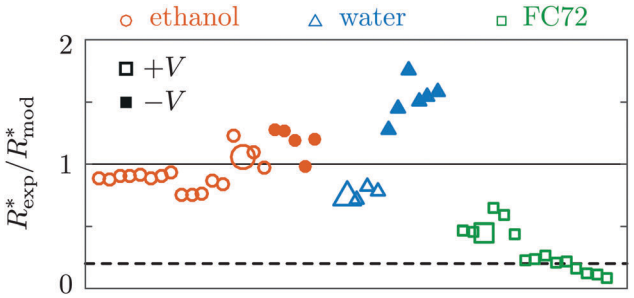

Fig. 6 Escape radius of the droplet (just before impact) in repeated experiments at various voltages (±(2–5) kV) and temperatures (120–300 °C), normalized by the predicted critical radius R^* given by eqn (8). For the dashed line the low dielectric constant of FC72 was taken into account. The large symbols correspond to the representative cases shown in Fig. 3.

charge is proportional to R^2, which, as the droplet shrinks, eventually overcomes the downward gravitational force proportional to R^3. The critical radius R^* for which this occurs can be estimated by balancing $F_g = -mg$ with $F_e \approx Q_d V_s/d$, leading to

$$R^* = \frac{\pi^2}{2}\frac{\varepsilon_0 V_s^2}{\rho g d^2}. \quad (8)$$

As shown in Fig. 6 this expression predicts the escape radius reasonably well (within about 50%) in a series of experiments done at various voltages and temperatures, and with different liquids. In the case of FC72 an additional prefactor $f = (\varepsilon_r - 1)/(\varepsilon_r + 2) \approx 0.2$ is required (dashed line) to take into account the liquid's low dielectric constant $\varepsilon_r \approx 1.7$ (as will be discussed in Section 6).

What remains to be explained are the details of the dribbling motion, such as the (sudden) increases and decreases in amplitude. To this end we look at the total change in potential energy ΔU during each jump. This energy can be calculated in two ways: one way is to assume that air drag is negligible and invoke conservation of energy, so that ΔU is equal to the kinetic energy K_0 with which the droplet leaves the surface. Another way is to use the inferred charge to directly calculate $U_m = mgY_m + U_e(Y_m)$ at the jumping maximums Y_m and to subtract the corresponding values U_0 of the droplet close to the surface. As shown in Fig. 3(a) (bottom panel) these independent energy measures give practically the same result, confirming that air drag can safely be neglected and at the same time validating our charge extraction method. For most parts of the trajectory the energy decreases after each rebound. For these low impact velocities this is likely due to dissipation associated with the oscillatory motion of the droplet after impact.[30,31] Interestingly, there is occasionally a sudden increase in energy. Comparing top and bottom panels in Fig. 3(a) one can see that these boosts in energy correlate with the sudden increases in jumping amplitude in the initial stage (stage I). We do not know the precise origin of these energy injections, but it could be related to the electro-capillary instability described in the previous section. Although the injections always seem to occur, their timing varies in repeated experiments under the same conditions. In the final stage (stage II), when the discharge

occurs in well defined steps, the droplet's energy decreases almost monotonically. At first sight this may seem at variance with the overall increasing jumping amplitude, but this is not the case. Both the gravitational and electric field contributions to the potential energy make that smaller droplets can jump higher with the same energy. In the final stage the dissipation rate is not high enough to counteract this effect. Here the amplitude drops at every discharge, as these events cause the potential energy to shift up for the same height.

In a previous study it was found that even without an external electric field, Leidenfrost droplets display a surprising (quasi) elastic bouncing behavior.[31] It was argued that the droplet finds a jumping mode in which energy dissipation is least, occurring when its oscillation time $t_R \approx \pi\sqrt{\rho R^3/(2\gamma)}$ becomes similar to the free fall time $t_f \approx \sqrt{2h/g}$. Solving $t_R = t_f$ for the fall height h, gives $h = \pi^2 g^2 \rho R^3/(4\gamma)$. This can also be rewritten as a condition on the kinetic energy by using that $mv^2/2 \approx mgh$, with v the velocity of the center of mass. Introducing the dimensionless Weber-number, $We = \rho R v^2/\gamma$, and Bond-number, $Bo = \rho g R^2/\gamma$, one finds the condition

$$We \approx \frac{\pi^2}{2} Bo^2. \quad (9)$$

If we evaluate this expression for our ethanol droplet, for which 1 mm $> R >$ 0.5 mm, we find $0.8 > We > 0.05$ and kinetic energies of 30 nJ $> K_0 >$ 0.5 nJ, which are indeed of the same order of magnitude as those found experimentally (Fig. 3(a)). Note that in the presence of charge on the droplet the oscillation frequency would change to $\omega^2 = [8\gamma - Q_d{}^2/(8\pi^2\varepsilon_0 R^3)]/(\rho R^3)$.[2] However, in the experiment considered here the amount of charge is still far (at about 10%) from the stability limit. We can therefore safely neglect the second term between the brackets. Another effect we need to consider is that the electric force will alter the free fall time. This could be incorporated by introducing an effective gravitational acceleration $g' \approx g - Q_d V_s/(md)$, which decreases from $g' \approx g$ just after deposition to $g' \approx 0$ when the droplet flies to the top electrode. However, in this final stage the free flight time is a lot longer than the time for the oscillations to damp out, so that the whole consideration above looses its validity anyhow. We can interpret eqn (9) as a kind of initial condition for the experiment, giving the typical kinetic energy before the electric forces take over.

6 Effect of liquid properties

In the model for predicting the droplet charge (eqn (4)) it was assumed that the droplet behaves as a perfect conductor. We expect this to work for liquids with a high relative permittivity $\varepsilon_r \gg 1$. In this section we will discuss results for water, which has a high permittivity of $\varepsilon_r \approx 55$, and perfluorohexane (FC72), which has an extremely low permittivity of $\varepsilon_r \approx 1.7$. Ethanol lies in between with a permittivity of about $\varepsilon_r \approx 19$. In Fig. 3 a typical result for water (V_s = 3 kV, T = 270 °C) is shown next to that for FC72 (V_s = 2.5 kV, T = 120 °C). It can be immediately seen that the behavior for the two liquids is quite different. The water droplet mostly stays close to the surface and takes one big leap near the end, while the FC72 droplet at some point starts to jump progressively higher, as was also observed for the ethanol droplets. The water droplet displays three clear charge steps, with each step starting on the line predicted by eqn (4). The duration of these charge plateaus is about 6 seconds in this case. In this time the droplet shrinks by about ΔR = 0.06 mm. Again taking $H \sim 10$ μm (which also turns out to be a good estimate for the water droplets) we find that the droplet voltage decreases by about $V_d = 1.1 V_s \Delta R/d \approx 28$ V before each discharge. About 5 times more than in the case of the ethanol droplet. This can be understood from the fact that for the water droplet the radius a of the flattened area during rebound is significantly smaller than R (see Fig. 3(b)). Because the droplet here bounces with a small amplitude and velocity, this flattening is dominated by gravity and can be estimated as $a/R \approx \sqrt{Bo} = R\sqrt{\rho g/\gamma} \approx 0.2$ (see also Appendix C).[32,33] According to eqn (7) we have $V_c \propto 1/a$, so that this indeed gives rise to a factor of 5 in the critical voltage compared to ethanol, for which we set $a = R$. The FC72 droplet shows just a single charge plateau, starting about 2 seconds before impact. During this same period it also starts to escape. Although this behavior is similar to what was found for ethanol droplets, the amount of charge is about two orders of magnitude lower. One order of magnitude can be explained by the smaller radius of the droplet. Eqn (4) would predict a charge of about 8×10^{-12} C for the droplet radius at the start of the plateau. To understand why the amount of charge is even smaller, we have to take into account the extremely low dielectric permittivity of FC72. Eqn (4) was derived by calculating the polarization of a perfectly conducting bi-sphere. This polarization was found to be about twice as large as that of a single sphere in the same electric field. It is well known that the polarization of a single dielectric sphere can be obtained directly from that of a single conducting sphere by multiplying the latter with a factor $f = (\varepsilon_r - 1)/(\varepsilon_r + 2)$.[34] Approximately the same factor will apply to the bi-sphere case. For ethanol and water this factor leads to a negligible correction, but for FC72, with $\varepsilon_r \approx 1.7$, one finds $f \approx 0.2$, explaining the low amount of charge observed. In Fig. 3(d) we took this factor into account in the comparison between the inferred charge (dots) and the model (dashed line). Had we not done this, then the line would lie outside the field of view. Similarly, this factor is necessary to understand the escape radii plotted in Fig. 6.

The above considerations imply that for FC72 also the formulas used for inferring the charge and potential energy (eqn (2) and (3)) are inaccurate, because the coefficients c_{ij} were calculated for perfect conductors. This error will occur mainly through the estimation of second order forces due to image charges, and may explain for example why the charge plateau for FC72 does not seem to be perfectly horizontal in Fig. 3(d) (this would also happen for water and ethanol in the simple point charge approximation).

7 Effect of electrode polarity

In the experiments described so far the top electrode was set to a positive voltage with respect to the grounded plate, so that the droplet attained a net negative charge. Fig. 7 (top) shows the

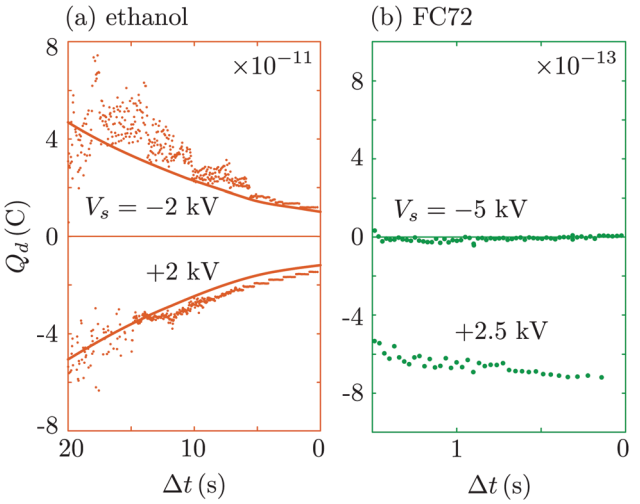

Fig. 7 Evolution of the charge on (a) ethanol droplets and (b) FC72 droplets trapped under either a negatively (top panels) or a positively charged electrode (bottom panels). While for ethanol the behavior is symmetric, FC72 does not obtain any positive charge, even for electrode voltages as low as −5 kV.

results of two experiments, one with ethanol (a) and one with FC72 (b), in which the voltage on the top electrode was set to a negative value (so that the droplets would get a positive charge). For comparison similar experiments for which the voltage was positive are also plotted (bottom).

While ethanol droplets behave practically the same for positive and negative voltage (as does water), FC72 droplets show an interesting asymmetric behavior under polarity reversal. The FC72 droplet seems to be unable to obtain any net positive charge. To trap the droplet under these neutral conditions we had to increase the magnitude of the voltage to at least $|V_s| = 5$ kV, and even then the droplet often rolled off the plate. This asymmetric charging behavior of FC72 is likely related to the chemically inert nature of this fluor-rich fluid. Similar to a Teflon-rod that is charged by rubbing, FC72 prefers to hold a negative charge.

8 Approaching the charging limit

To observe the progressive increase in jumping amplitude, the voltage on the top electrode has to be high enough to overcome the loss in height due to energy dissipation (see Section 5). However, if the voltage is too high, the spherical shape of the droplet becomes unstable with respect to a conical shape.[5] For ethanol and water this happens around $V_s \gtrsim 4$ kV in our setup.

Fig. 8 shows some snapshots of these instabilities. Initially, both the water and ethanol droplet developed a Taylor cone at their upper surfaces. For the ethanol droplet this cone quickly destabilized and started to eject small droplets. In the same recording the ethanol droplet occasionally stretched into a thin filament bridging the whole gap. This filament remained stable for a while, and then broke up into several smaller droplets, leading to a very irregular behavior. For the water droplet no ejection was observed, instead the tension was released by a violent electrical discharge striking the drop's sharp tip.

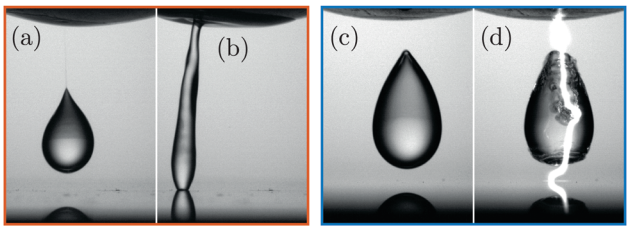

Fig. 8 Instabilities observed for (a and b) ethanol and (c and d) water droplets at voltage differences above 4 kV. In (a) the ethanol droplet developed a sharp cone from which small droplets are ejected. A few bounces later (b) it temporary formed a vertical bridge between the top electrode and the hot bottom plate, still hovering on a vapor film. Also the water droplet (c) first developed a cone, but in this case (d) the electrical tension is released by a violent discharge that ruptures the drop.

9 Conclusion and outlook

Small Leidenfrost droplets in a vertical electric field of strengths between 2 and 5 kV cm^{-1} display a surprising regular and repeatable dribbling motion, in which they escape from the hot surface by jumping progressively higher. We have related this behavior to the electrical and gravitational forces acting respectively on the charge and mass of the droplet. As the droplet shrinks due to evaporation, the charge on the droplet decreases in a step like manner to remain proportional to R^2. Eventually the upward electrical force will therefore always dominate over the gravitational force, which is proportional to R^3. The discrete discharge events were attributed to an electro-capillary instability in the vapor gap, occurring each time the electrical potential of the droplet reaches a critical value.

In an analysis of the potential and kinetic energies of the dribbling droplets we have found that for most parts of the drop's motion the jumping energy slowly decreases in time. However, the droplet occasionally receives a boost, helping it to escape. These sudden energy injections will be an interesting subject for future research (What is their (electro-capillary) origin? How does their frequency and strength depends on the control parameters? *etc.*) In the final stage, the decrease in potential energy due to evaporation is by itself enough to allow the jumping amplitude to increase.

The theoretical approach employed in this work, using capacitance coefficients to calculate potentials, forces and energies, can be extended to any geometry. This opens up the possibility to design electrical circuitry to trap and steer the hyper-mobile Leidenfrost droplets (*e.g.* in microfluidic devices). Furthermore, the method of inferring the charge from the droplet's trajectory offers an easy way to study the basic charging properties of a liquid or the insulation properties of its vapor.

Appendices

A Horizontal trapping potential

The most basic electrode configuration for creating a vertical electrical field would be two parallel plates. However, practically it is more convenient to let one of the electrodes have a slight curvature. In this case there is no need to align the electrodes and it ensures that a charged droplet experiences a slight trapping force,

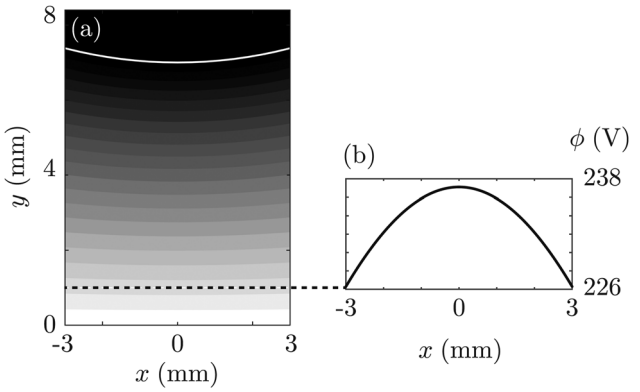

Fig. 9 (a) Electrical potential between a conducting sphere of V_s = 2 kV (black) and a grounded plate (white). (b) Horizontal slice through the field in (a) showing the weak trapping potential close to the plate.

keeping it in the field of view. The electrical potential between a sphere of radius R_s with its center a distance d_c above a plate can be calculated numerically through a summation over image charges. The positions y_n and magnitudes q_n of these virtual point charges in the top electrode are given by the recursive relation:

$$\begin{aligned} y_1 &= d_c \\ y_n &= d_c - \frac{{R_s}^2}{d_c + y_{n-1}} \\ q_1 &= R_s V_s \\ q_n &= \frac{R}{d_c + y_{n-1}} q_{n-1} \quad (n = 2, 3, \dots) \end{aligned} \tag{10}$$

Another set of charges with the same magnitude but of opposite sign, are to be placed below the plate, mirrored with respect to the plate surface. The potential field $\phi(x,y)$ is then simply given by summing over the potentials $\phi_n(x,y) = \pm q_n/r_n(x,y)$, with r_n the distance to the point charge. Fig. 9(a) shows a contour plot of the potential calculated in this way, with V_s = 2 kV. To extract the trapping potential (at a certain height Y_{CM}) we take a horizontal slice $\phi(x,Y_{CM})$, as shown in Fig. 9(b). The potential energy is given by $U(x) = Q_d\phi(x)$. For small motions about the center this potential is approximately harmonic and we can define a spring constant as

$$k(y) \equiv Q_d \frac{\partial^2 \phi}{\partial x^2}. \tag{11}$$

A droplet with mass m and charge Q_d will then oscillate with angular frequency

$$\omega^2 = \frac{k}{m} = \frac{Q_d}{m} \frac{\partial^2 \phi}{\partial x^2}. \tag{12}$$

In each experiment all quantities except Q_d are known, thus providing an other method to extract the charge on the droplet. The result of such an analysis is shown in Fig. 10. Although the inferred charge is consistent with that found from the vertical motion, the horizontal motion is less regular, resulting in a large scatter.

B Capacitance and force coefficients

To infer the charge on the droplet through eqn (1) one needs to know the electrical force F_e on the droplet as a function of its position and size. Substituting eqn (2) into eqn (3) one obtains:

$$F_e = -\partial_{Y_{CM}} U = f_{dd} {Q_d}^2 + f_{ds} Q_d V_s + f_{ss} {V_s}^2, \tag{13}$$

with the 'force coefficients' $f_{ij} = f_{ij}(Y_{CM}, R)$ related to the capacitance coefficients as $f_{dd} = -\partial_Y(1/c_{dd})/2$, $f_{ds} = \partial_Y(c_{ds}/c_{dd})$ and $f_{ss} = \partial_Y(c_{ss} - {c_{ds}}^2/c_{dd})/2$. In first approximation the force acting on a charged droplet is given by $F_e = Q_d V_s/d$, which assumes that the droplet can be treated as a point in an external electrical field of strength V_s/d. The corresponding force coefficients would be $f_{dd} = f_{ss} = 0$, and $f_{ds} = 1/d$. Although this approximation gives already quite a good estimate of the amount of charge on the droplet, it fails when the droplet is very close to the plate.

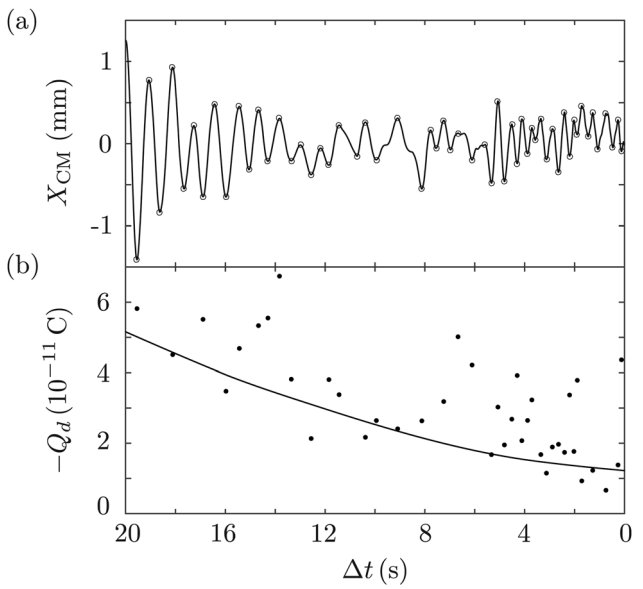

Fig. 10 (a) Horizontal motion of the center of mass of a charged ethanol droplet in the trapping potential and (b) the charge inferred from this oscillatory motion.

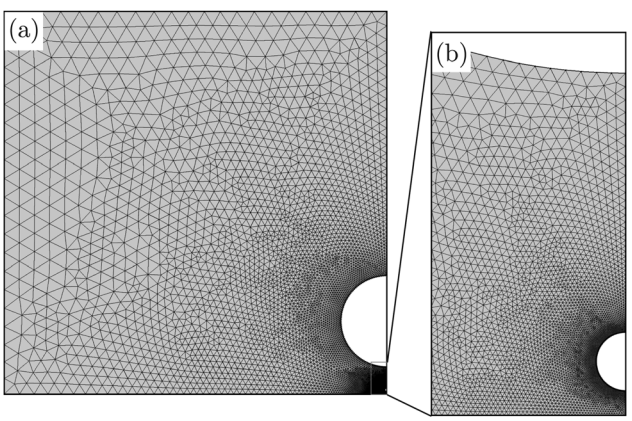

Fig. 11 Geometry and mesh used to calculated the force and capacitance coefficients with COMSOL. (a) Overview of the (axisymmetric) computational domain with spherical top electrode clearly visible. (b) Magnification of the gap between the top electrode and the plate, with the droplet in between. The surfaces of the droplet and the top electrode have a fine mesh.

Furthermore, the charge plateaus are not horizontal in this approximation, giving the wrong impression that the charge here slowly increases or decreases. To circumvent these errors and to check the analytical expressions used in the main text, we used the electrostatics module of COMSOL (version 5.0) to directly calculate both the capacitance and force coefficients in our setup. Fig. 11 shows the typical geometry and mesh used in these calculations. To calculate for example the capacitance coefficient c_{ds}, the voltage of the top electrode was set to 1 V, while the droplet was grounded (*cf.* Fig. 4). c_{ds} is then given by the total amount of surface charge accumulated on the conductor that represents the droplet. To obtain sufficient accuracy for performing these integrals, the mesh was extra refined on the surfaces of the conductors.

These calculations were repeated for a range of droplet heights H and radii R, to obtain a fine grid of coefficients $c_{ij}(H,R)$ covering all the radii and heights found in the experiments. Values in between the grid points were obtained through interpolation. To give an idea of their behavior, Fig. 12 shows the coefficients as a function of H, and a fixed radius of $R = 0.6$ mm. In eqn (5) we used approximations for c_{dd} and c_{ds} to calculated the electrical potential of the drop when it is close to the surface ($H \ll R$). In Fig. 12 these approximations are shown as dashed lines. They indeed approach the correct values in the limit $H \to 0$.

The force coefficients can in principle be obtained from the variation of capacitance coefficients with H by taking the appropriate combinations and then taking the derivative. However, it turns out that doing this numerically leads to some errors, especially for f_{ss} which is calculated as $f_{ss} = \partial_H(c_{ss} - c_{ds}^2/c_{dd})/2$. To circumvent this numerical differentiation, we also directly calculated the force coefficients by treating the droplet as a floating potential with a fixed charge $Q = 1$ C or 0 C (and, as before, with the top electrode set to 1 V or 0 V) and directly calculating the net force exerted by the field on the surface charges. The plots in Fig. 12 show both the coefficients obtained through differentiation (black dots) and through direct calculation (gray lines). For f_{dd} and f_{ds} the two methods practically overlap, but for f_{ss} the direct method performs significantly better.

C Vapor film thickness

Our prediction for the critical discharge voltage of the droplet, eqn (7), relies on an estimation of the minimum height of the vapor gap below the droplet during a rebound. For this estimation we will follow a similar procedure as outlined in Biance *et al.*[26] for droplets in a gravitational field. We then extend this approach to droplets impacting with a finite velocity to see whether it is the impact force or the gravitational force which dominates in our case. The situation is sketched in Fig. 13.

When a millimetric droplet sits on a solid surface (with or without vapor in between) the bottom of the droplets gets indented by the small amount:[32]

$$\delta_g \sim \frac{\rho g R^3}{\gamma} = R\mathrm{Bo}, \tag{14}$$

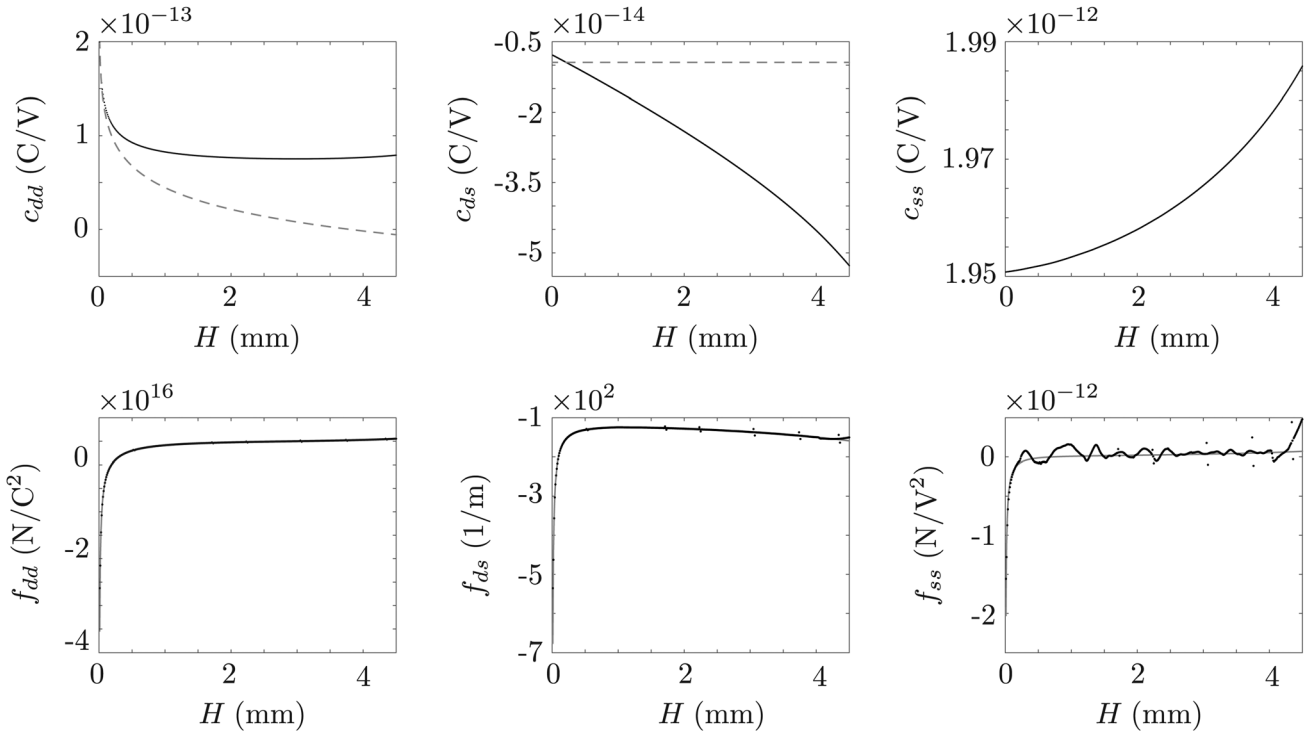

Fig. 12 Capacitance coefficients c_{ij} and force coefficients f_{ij} as a function of the gap between the droplet and the plate H, for a fixed radius of $R = 0.6$ mm. The black dots are the calculated coefficients (it is hard to see separate dots because of the fine grid of points). For c_{dd} and c_{ds} also analytical asymptotic solutions for $H/R \to 0$ are shown. The force coefficients were calculated both from the capacitance coefficients (black dots) and directly by integrating the force in the simulation (gray lines).

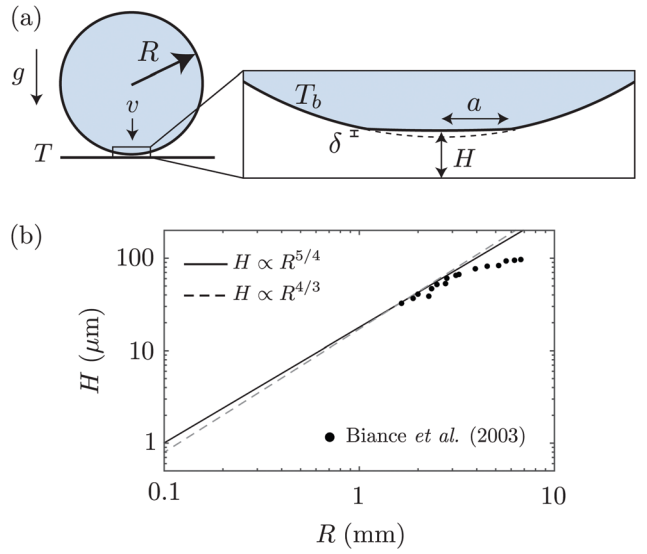

Fig. 13 (a) Sketch of a small droplet that deforms upon impact with a solid surface. (b) Minimum height of the vapor gap when gravity dominates inertia. Dots show experiments from Biance *et al.* and the lines represent different scaling expressions, eqn (18) (solid line) and eqn (8) from Biance *et al.* (dashed line). For both lines the pre-factor was adjusted to make the lines go through the first data point.

so that the decrease in potential energy due to the lowering of the center of mass is balanced by an increase in the surface energy. From the spherical geometry of the droplet it follows that the radius of the flattened area is:

$$a \sim \sqrt{R\delta_g} = R\mathrm{Bo}^{1/2} \tag{15}$$

The flattening of the bottom locally exposes the Laplace pressure of the droplet. In the solid this pressure is supplied by a small elastic deformation. When there is a vapor film between the solid and the droplet, the same pressure has to be built up in the vapor. This is possible when the gap becomes so small that viscous forces in the vapor become important. The flow in the gap can then be shown to be equivalent to the classical lubrication problem of a squeezing flow below a flat disk of radius a moving down with the velocity of the generated vapor:

$$v_v \sim \frac{k_v \Delta T}{L\rho_v H}, \tag{16}$$

where k_v is the thermal conductivity of the vapor and L the latent heat of evaporation. The maximum lubrication pressure for the squeezing flow scales as:

$$p_\mu \sim \frac{\mu_v v_r a}{H^2} \sim \frac{\mu_v v_v a^2}{H^3}, \tag{17}$$

where $v_r \sim v_v a/H$ is the radial flow velocity and μ_v is the dynamic viscosity of the vapor. This pressure has to balance the Laplace pressure $p_\gamma \sim \gamma/R$. Setting $p_\mu \sim p_\gamma$, and using eqn (14)–(17) we find:

$$\frac{H}{R} \sim \left(\frac{k_v \Delta T R \mu_v \rho g}{L\rho_v \gamma^2}\right)^{1/4}. \tag{18}$$

This expression is similar to eqn (8) in Biance *et al.*, except that we here find an exponent of 1/4 instead of 1/3 on the dimensionless term between brackets. The difference is that in the former work, it was assumed that heat transfer to the whole droplet surface contributes to the vapor flow in the gap. In Fig. 13b we reproduced the experimental data and eqn (8) (dashed line) from Biance *et al.*, and also plot eqn (18) derived above (solid line). The pre-factors were adjusted so that both lines go through the first experimental point, we find a pre-factors of 2.5 for the former and 0.75 for the latter, which seems to favour eqn (18). However, given these pre-factors the correct slope cannot be inferred from the measurements, and for the radii we are interested in here, $R \sim 1$ mm, both lines predict a similar film thickness of about $H \approx 20$ μm. For droplets larger than about $R = 3$ mm the deformations are no longer small and the droplets cannot be assumed spherical, so that the models do not work in this regime.

When the droplet has a finite impact velocity v, its momentum will provide an additional force that pushes the droplet down. If we suppose that the droplet decelerates over a distance δ, we can interpreted this in the frame of reference of the droplet as an effective gravitational acceleration:

$$g' \sim \frac{v^2}{\delta}. \tag{19}$$

Using this in eqn (14), and solving for δ, gives:

$$\delta_v \sim \sqrt{\frac{\rho v^2 R^3}{\gamma}} = R\mathrm{We}^{1/2} \tag{20}$$

Note that the same result is found by comparing the kinetic energy $\sim\rho R^3 v^2$ to the energy associated with the small deformation of the surface $\sim\gamma\delta^2$. Comparing eqn (14) and (20) one obtains that the transition from a gravity to an inertia dominated regime occurs for:

$$\mathrm{We} \sim \mathrm{Bo}^2. \tag{21}$$

Coincidentally this condition corresponds precisely to that for the natural jumping mode of small Leidenfrost droplets (*cf.* eqn (9)). This means that in our experiment the droplets are always found in this transitional regime, and it does not matter much which scale is used to estimate H.

Acknowledgements

We thank Gert-Wim Bruggert, Martin Bos and Bas Benschop for their technical assistance, Leen van Wijngaarden, Andrea Prosperetti and Detlef Lohse for useful suggestions and Rianne de Jong for helping out with the preliminary experiments. This project was financed by an ERC Advanced Grant.

References

1 W. Gilbert, De Magnete, Book 2, (Trans. by S. P. Thompson, 1900), 1600, p. 55.
2 J. W. Strutt, *Philos. Mag. Ser. 5*, 1882, **14**, 184–186.
3 R. A. Millikan, *Phys. Rev.*, 1913, **2**, 109–143.
4 J. Zeleny, *Phys. Rev.*, 1917, **10**, 1–6.
5 G. Taylor, *Proc. R. Soc. London, Ser. A*, 1964, **280**, 383–397.
6 W. G. Armstrong, *Electr. Eng.*, 1893, 154–155.

7 A. G. Marín and D. Lohse, *Phys. Fluids*, 2010, **22**, 122104.
8 G. Taylor, *Proc. R. Soc. London, Ser. A*, 1969, **313**, 453–475.
9 G. Riboux, A. G. Marín, I. G. Loscertales and A. Barrero, *J. Fluid Mech.*, 2011, **671**, 226–253.
10 J. C. Bird, W. D. Ristenpart, A. Belmonte and H. A. Stone, *Phys. Rev. Lett.*, 2009, **103**, 164502.
11 W. D. Ristenpart, J. C. Bird, A. Belmonte, F. Dollar and H. A. Stone, *Nature*, 2009, **461**, 377–380.
12 J. G. Leidenfrost, *De aquae communis nonnullis qualitatibus tractatus*, Ovenius, Duisburg, 1756.
13 M. Le Merrer, C. Clanet, D. Quéré, E. Raphaël and F. Chevy, *Proc. Natl. Acad. Sci. U. S. A.*, 2011, **108**, 15064–15068.
14 H. Linke, B. J. Alemán, L. D. Melling, M. J. Taormina, M. J. Francis, C. C. Dow-Hygelund, V. Narayanan, R. P. Taylor and A. Stout, *Phys. Rev. Lett.*, 2006, **96**, 154502.
15 G. Lagubeau, M. Le Merrer, C. Clanet and D. Quéré, *Nat. Phys.*, 2011, **7**, 395–398.
16 A. G. Marín, D. Arnaldo del Cerro, G. R. B. E. Römer, B. Pathiraj, A. Huis in 't Veld and D. Lohse, *Phys. Fluids*, 2012, **24**, 122001.
17 K. Piroird, B. D. Texier, C. Clanet and D. Quéré, *Phys. Fluids*, 2013, **25**, 032108.
18 D. Quéré, *Annu. Rev. Fluid Mech.*, 2013, **45**, 197–215.
19 F. Celestini and G. Kirstetter, *Soft Matter*, 2012, **8**, 5992–5995.
20 A. Shahriari, J. Wurz and V. Bahadur, *Langmuir*, 2014, **30**, 12074–12081.
21 R. de Ruiter, A. M. Pit, V. M. de Oliveira, M. H. G. Duits, D. van den Ende and F. Mugele, *Lab Chip*, 2014, **14**, 883–891.
22 B. Ahn, K. Lee, R. Panchapakesan and K. W. Oh, *Biomicrofluidics*, 2011, **5**, 024113.
23 J. C. Maxwell, *A Treatise on Electricity and Magnetism*, Clarendon Press, Oxford, UK, 3rd edn, 1891, vol. 1, (Reprinted by Dover 1954).
24 W. E. Smith and J. Rungis, *J. Phys. E: Sci. Instrum.*, 1975, **8**, 379.
25 J. Lekner, *Proc. R. Soc. A*, 2012, **468**, 2829–2848.
26 A. Biance, C. Clanet and D. Quéré, *Phys. Fluids*, 2003, **15**, 1632.
27 D. Marić, J. Sivoš, N. Škoro, G. Malović and Z. L. Petrović, *31st ICPIG E-b. Abstr.*, 2013.
28 J. H. Snoeijer, P. Brunet and J. Eggers, *Phys. Rev. E: Stat., Nonlinear, Soft Matter Phys.*, 2009, **79**, 1–13.
29 G. Taylor, *Proc. R. Soc. London, Ser. A*, 1950, **201**, 192–196.
30 D. Richard and D. Quéré, *Europhys. Lett.*, 2000, **50**, 769.
31 A.-L. Biance, F. Chevy, C. Clanet, G. Lagubeau and D. Quéré, *J. Fluid Mech.*, 2006, **554**, 47–66.
32 L. Mahadevan and Y. Pomeau, *Phys. Fluids*, 1999, **11**, 2449.
33 P. Aussillous and D. Quéré, *Nature*, 2001, **411**, 924–927.
34 L. D. Landau, E. M. Lifshitz and L. P. Pitaevskii, *Electrodynamics of Continuous Media (Course of Theoretical Physics)*, Butterworth-Heinemann (Elsevier), Oxford, UK, 2nd edn, 1984, vol. 8.

